K. M. Shen for helpful discussions and communications. Experimental studies were supported by the Center for Emergent Superconductivity, an Energy Frontier Research Center, headquartered at Brookhaven National Laboratory (BNL) and funded by the U.S. Department of Energy under grant DE-2009-BNL-PM015, as well as by a Grant-in-Aid for Scientific Research from the Ministry of Science and Education (Japan) and the Global Centers of Excellence Program for Japan Society for the Promotion of Science. C.K.K. acknowledges support from the FlucTeam program at BNL under contract DE-AC02-98CH10886. J.L. acknowledges support from the Institute for Basic Science, Korea. I.A.F. acknowledges support from Fundação para a Ciência e a Tecnologia, Portugal, under fellowship number SFRH/BD/60952/2009. S.M. acknowledges support from NSF grant DMR-1120296 to the Cornell Center for Materials Research. Theoretical studies at Cornell University were supported by NSF grant DMR-1120296 to Cornell Center for Materials Research and by NSF grant DMR-0955822. The original data are archived by Davis Group, BNL, and Cornell University.

Supplementary Materials
www.sciencemag.org/content/344/6184/612/suppl/DC1
Materials and Methods
Supplementary Text
Figs. S1 to S9
References (*42*–*45*)
Movies S1 and S2

21 November 2013; accepted 20 March 2014
10.1126/science.1248783

Direct, Nonoxidative Conversion of Methane to Ethylene, Aromatics, and Hydrogen

Xiaoguang Guo,[1] Guangzong Fang,[1] Gang Li,[2,3] Hao Ma,[1] Hongjun Fan,[2] Liang Yu,[1] Chao Ma,[4] Xing Wu,[5] Dehui Deng,[1] Mingming Wei,[1] Dali Tan,[1] Rui Si,[6] Shuo Zhang,[6] Jianqi Li,[4] Litao Sun,[5] Zichao Tang,[2] Xiulian Pan,[1] Xinhe Bao[1]*

The efficient use of natural gas will require catalysts that can activate the first C–H bond of methane while suppressing complete dehydrogenation and avoiding overoxidation. We report that single iron sites embedded in a silica matrix enable direct, nonoxidative conversion of methane, exclusively to ethylene and aromatics. The reaction is initiated by catalytic generation of methyl radicals, followed by a series of gas-phase reactions. The absence of adjacent iron sites prevents catalytic C-C coupling, further oligomerization, and hence, coke deposition. At 1363 kelvin, methane conversion reached a maximum at 48.1% and ethylene selectivity peaked at 48.4%, whereas the total hydrocarbon selectivity exceeded 99%, representing an atom-economical transformation process of methane. The lattice-confined single iron sites delivered stable performance, with no deactivation observed during a 60-hour test.

The challenge of converting natural gas into transportable fuels and chemicals (*1*) has been spurred by several emerging industrial trends, including rapidly rising demand for H_2 (for upgrading lower-quality oils) and a global shortage of aromatics caused by shifting refinery targets toward gasoline. Light olefins, which are key chemical feedstocks, are currently made from methanol, which itself is made through multistage catalytic transformations via syngas (a mixture of H_2 and CO) (*2*, *3*), although there is also ongoing research to convert syngas directly to light olefins (*4*, *5*). However, in all such approaches, either CO or H_2 is needed to remove oxygen from CO, resulting in a carbon-atom utilization efficiency below 50%. Despite their low efficiency, high capital and production costs, and enormous CO_2 emissions, syngas routes dominate current and near-term industrial practices for natural gas conversion (*6*, *7*).

Direct conversion of CH_4 is potentially more economical and environmentally friendly but is challenging because CH_4 exhibits high C–H bond strength (434 kJ/mol), negligible electron affinity, large ionization energy, and low polarizability (*8*). In the pioneering work of Keller and Bhasin in the early 1980s, CH_4 was activated with the assistance of oxygen (*9*). This finding initiated a worldwide research surge to explore the high-temperature (>1073 K) oxidative coupling of methane (OCM) to C_2 hydrocarbons (*10*, *11*). Hundreds of catalytic materials have since been synthesized and tested, principally during the 1990s, as well as in recent years. Unfortunately, the presence of O_2 leads irreversibly to overoxidation, resulting in a large amount of the thermodynamically stable end-products CO_2 and H_2O. Thus, the carbon utilization efficiency of OCM remains relatively low (*12*, *13*). Slow progress in discovering new catalysts to circumvent this problem has hindered further development, and no economically viable process has been put into practice so far.

In a recent report, elemental sulfur was used as a softer oxidant than O_2 (*14*): For a 5% CH_4/Ar mixture at 1323 K, the best catalyst, PdS/ZrO_2, gave a CH_4 conversion of ~16% and ethylene selectivity near 20%, albeit at the expense of the by-products CS_2 and H_2S (*14*). In contrast, the bifunctional catalysts based on Mo/zeolites catalyze CH_4 conversion to aromatics (benzene and naphthalene) nonoxidatively, thereby avoiding CO_2 formation (*15*–*18*). CH_4 is activated on the metal sites forming CH_x species, which dimerize to C_2H_y. Subsequent oligomerization on the acidic sites located inside the zeolite pores yields benzene and naphthalene, as well as copious amounts of coke (*19*–*21*). Commercial prospects for this process are further hampered by the instability of zeolites at the very high reaction temperatures.

To achieve direct conversion of CH_4 efficiently, the challenges lie in cleaving the first C–H bond while suppressing further catalytic dehydrogenation, avoiding both CO_2 generation and coke deposition. We report that these conditions can be met using lattice-confined single iron sites embedded in a silica matrix. These sites activate CH_4 in the absence of oxidants, generating methyl radicals, which desorb from the catalyst surface and then undergo a series of gas-phase reactions to yield ethylene, benzene, and naphthalene as the only products (with ethylene dominating at short space-times for a selectivity of ~52.7% at 1293 K). A methane conversion as high as 48.1% is achieved at 1363 K.

The catalysts were obtained by fusing ferrous metasilicate with SiO_2 at 1973 K in air and from commercial quartz, followed by leaching with aqueous HNO_3 and drying at 353 K (*22*). The resulting catalyst was designated 0.5% Fe©SiO_2 (© denotes confinement and here represents a catalyst characterized by the lattice-confined single iron sites embedded within a silica matrix). It contained 0.5 weight percent (wt %) Fe and had a Brunauer–Emmett–Teller surface area of <1 m^2/g. The catalyst was activated in a fixed-bed microreactor in the reaction atmosphere [90 volume percent (vol %) CH_4/N_2] at 1173 K. The effluent was analyzed by online gas chromatography (GC). At 1223 K, CH_4 conversion was 8.1% (Fig. 1A) and increased with temperature, exceeding 48.1% at 1363 K (Fig. 1B). Only ethylene, benzene, and naphthalene were produced; neither coke nor CO_2 was detected, despite the relatively high reaction temperature. A single-pass yield of 48% hydrocarbons is achieved at 1363 K and 21.4 liters per gram of catalyst (gcat) per hour. Selectivities vary from 40.9 to 52.1% for ethylene, 21.0 to 29.1 for benzene, and 23.6 to 38.2% for naphthalene, over the investigated temperature range (1223 to 1363 K).

By comparison, a blank experiment (an empty reactor with no catalyst) under the same conditions showed a CH_4 conversion of only 2.5%, and 95% of the product was coke (Fig. 1A). A test with unmodified SiO_2 as the catalyst yielded virtually

[1]State Key Laboratory of Catalysis, Dalian Institute of Chemical Physics, Chinese Academy of Sciences, Dalian 116023, People's Republic of China. [2]State Key Laboratory of Molecular Reaction Dynamics, Dalian Institute of Chemical Physics, Chinese Academy of Sciences, Dalian 116023, People's Republic of China. [3]State Key Laboratory of Fine Chemicals, Institute of Coal Chemical Engineering, School of Chemical Engineering, Dalian University of Technology, Dalian 116012, People's Republic of China. [4]Beijing National Laboratory for Condensed Matter Physics, Institute of Physics, Chinese Academy of Sciences, Beijing 100190, People's Republic of China. [5]Nano-Pico Center, Key Laboratory of Micro-Electro-Mechanical System (MEMS) of Ministry of Education, Southeast University, Nanjing 210096, People's Republic of China. [6]Shanghai Synchrotron Radiation Facility, Shanghai Institute of Applied Physics, Chinese Academy of Sciences, Shanghai 201204, People's Republic of China.
*Corresponding author. E-mail: xhbao@dicp.ac.cn

the same result (table S1) (*22*). Most notably, the use of 0.5 wt % Fe/SiO_2 as the catalyst (prepared with wet impregnation on amorphous SiO_2 with a high surface area, 348 m^2/g) (*22*) also led to high coke formation (>98%). We have varied the iron loadings, support materials, and preparation methods, which unfortunately do not preclude coke on iron nanoparticles (NPs). For example, coke remained the principal product (>50%) over 0.5% Fe/ZSM. 0.8% Fe/SiO_2 prepared by sol-gel method and 0.2% Fe/SiC (*22*) enhanced selective formation of hydrocarbons to some extent, but still with a considerable amount of coke (Fig. 1A).

Figure S1 (*22*) demonstrates that the reactivity of 0.5% Fe©SiO_2 was very reproducible. All mass balances are above 99%. At 1363 K, the space-time yields for ethylene, benzene, and naphthalene were 91, 18, and 9 mol $kgcat^{-1}$ $hour^{-1}$, respectively. Moreover, the process represents a new and sustainable approach to H_2 production because the by-products are high–value-added hydrocarbons (ethylene and aromatics) instead of coke and CO_2 (*23*, *24*). The yield of H_2 varies with the reaction conditions, and the concentrations in the effluent range from 10.9 to 51.2% (fig. 1D) (*22*).

Furthermore, the 0.5% Fe©SiO_2 catalyst was very stable, and no deactivation was observed during a 60-hour test at 1293 K (Fig. 1C). Methane conversion remained at ~32% throughout this long run. Selectivities to ethylene (52.7%), benzene (21.5%), and naphthalene (25.8%) were constant, and the total selectivity to these products remained >99%. The combination of atom-economy, high selectivity, and high conversion is notable, considering the rather low loading of Fe (0.5 wt %) and very low surface area (<1 m^2/g) of the SiO_2. Although noncatalytic pyrolysis of CH_4 has been extensively studied for light hydrocarbon synthesis, the product is dominated with acetylene accompanied by high coke formation (*25*–*27*). By comparison, the catalytically initiated reaction described here compares very favorably with other reported direct-conversion processes, including pyrolysis, OCM (*13*), and nonoxidative aromatization (*21*). Finally, because natural gas usually contains some ethane, we added 1 and 5 vol % ethane to the reactant stream. The presence of ethane substantially enhanced methane conversion (fig. S2) (*22*), and ethane is almost completely converted, although a small amount of coke is formed at 1173 K and a space velocity of 4.84 liter $gcat^{-1}$ h^{-1}.

The unprecedented efficiency of the catalytically initiated CH_4 conversion process is attributed to the high activity of the coordinatively unsaturated iron sites toward the C-H bond of CH_4 (*28*, *29*). The isolated nature of these sites, as evidenced by sub-angstrom–resolution high-angle annular-dark field (HAADF) scanning transmission electron microscopy (STEM) and in situ x-ray absorption near-edge spectroscopy (XANES), precludes surface C-C coupling and, hence, coke formation. Transmission electron microscopy indicates that in the fresh 0.5% Fe©SiO_2 catalyst, iron oxide NPs with a size of ~3 to 4 nm are distributed homogeneously throughout the SiO_2 matrix (fig. S3) (*22*). A STEM-HAADF image of the catalyst after reaction reveals many bright dots of atomic size scattered across the SiO_2 matrix, highlighted by the red circles in Fig. 2A. Each dot represents an individual Fe atom, considering the much lower contrast of Si and O in the HAADF image. This result suggests that the iron species are redistributed from the original oxide NPs to isolated atoms during catalyst activation.

This hypothesis is validated by the in situ XANES during activation. The near-edge spectrum of the catalyst is similar to that of Fe foil (Fig. 2B). In Fig. 2C, the Fourier-transformed k^3-weighted $\chi(k)$ function (where k is wave number) (*30*) shows that, after activation, the Fe-O scattering paths apparent in the spectrum of the fresh catalyst (line 1) have disappeared,

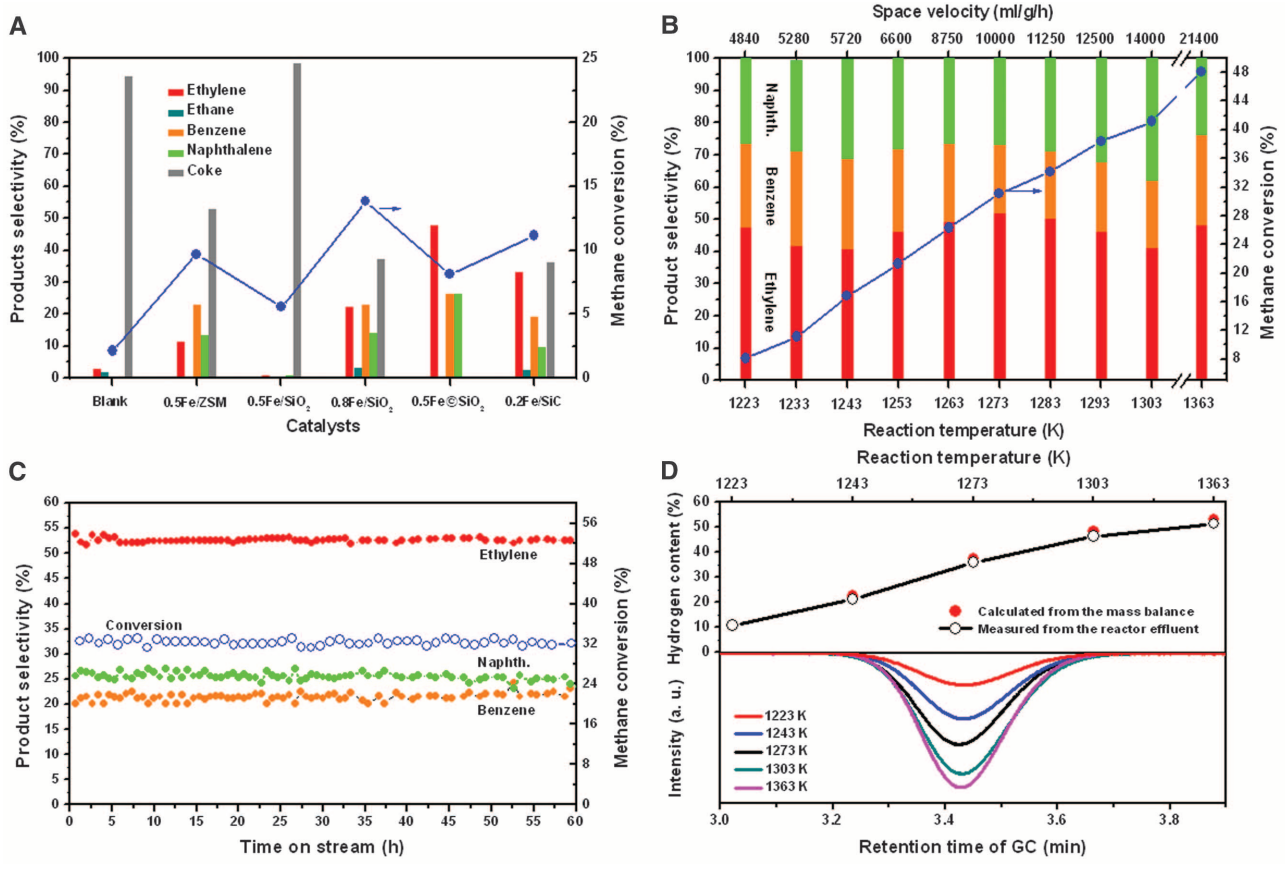

Fig. 1. Reaction performance. (**A**) Comparison of different catalysts at 1223 K and 4.84 liter $gcat^{-1}$ $hour^{-1}$. (**B**) Effect of reaction temperatures and space velocities on the 0.5% Fe©SiO_2 catalyst. Blue circles denote CH_4 conversion, whereas bars represent product selectivities. (**C**) Long-term stability test of 0.5% Fe©SiO_2 at 1293 K and 14.5 liter $gcat^{-1}$ $hour^{-1}$. (**D**) (Top) Hydrogen contents of the reactor effluent (open circles) and the calculated values (solid circles); (bottom) H_2 peaks in GC analysis normalized by the internal standard N_2 (*22*). a. u., arbitrary units.

whereas new scattering paths appear (line 2). They are assigned to Fe-C and Fe-Si paths, by comparison to the spectra of reference materials such as Fe_2O_3, $FeSi_2$, and iron carbides (*31*). In the presence of CH_4 above 1173 K, iron oxide species in the fresh 0.5% Fe©SiO_2 interact extensively with the support, becoming embedded in the silica matrix through bonding to Si and C atoms. Thus, these otherwise extremely reactive, coordinatively unsaturated iron atoms are stabilized and persist under the very harsh reaction conditions. No aggregation was observed, even after prolonged reaction for 60 hours.

In contrast, the 2- to 5-nm-sized iron NPs in 0.5% Fe/SiO_2 (fig. S5a) (*22*) after activation under the same conditions exhibit only a Fe–Fe bond (line 3 in Fig. 2, B and C). This result explains the extensive carbon deposition observed for 0.5% Fe/SiO_2, considering that iron NPs are widely used for the synthesis of carbon nanotubes (*32*). That process involves catalytic cleavage of C–H bonds and dissolution of carbon species into the iron lattice. Subsequent C-C coupling on an iron NP surface and crystallization from the supersaturated carbide solid solution drive the growth of nanotubes (*33*). However, under the harsh reaction conditions in the current reaction, 0.5% Fe/SiO_2 deactivates very rapidly, and iron NPs aggregated and grew to 20 to 30 nm after reaction (fig. S4b) (*22*). These results again highlight the crucial role played by the site isolation of the iron species in 0.5% Fe©SiO_2 in achieving high selectivity toward hydrocarbons and preventing coke formation.

Furthermore, density functional theory (DFT) calculations suggest that the most stable structure in the reactive atmosphere is an iron atom coordinated by one Si and two C atoms and is thus embedded within the SiO_2 matrix, as depicted in Fig. 3A and fig. S5. The calculated Fe–C and Fe–Si bond lengths are 1.6 and 2.4 Å, respectively, which are consistent with those estimated from extended x-ray absorption fine structure (EXAFS) (table S2) (*22*). This lattice-confined single iron site initiates CH_4 dehydrogenation by generating a •CH_3 radical, which subsequently releases from the surface with an energy barrier of 2.32 eV instead of undergoing further dehydrogenation or C-C coupling (fig. S5) (*22*). The Fe site is then exposed and becomes active for adsorption of a second methane molecule and release of another methyl radical, with energy barriers of 3.07 and 2.19 eV, respectively (Fig. 3A). Migration of H from C in Fe-C-Si sites to Fe involves a barrier of 0.58 eV. The resulting surface H species desorbs as H_2 with an energy barrier of 1.61 eV.

The intermediacy of methyl radicals was verified by online vacuum ultraviolet soft photoionization molecular-beam mass spectrometry (VUV-SPI-MBMS) (fig. S6) (*22*). Molecules were ionized with a 10.6-eV VUV lamp, which has an energy lower than the CH_4 ionization energy (12.6 eV). This allows detection of intermediate radicals and products (*34*, *35*). Figure 3B and its inset display all species detected at 1193 K. Methyl radicals,

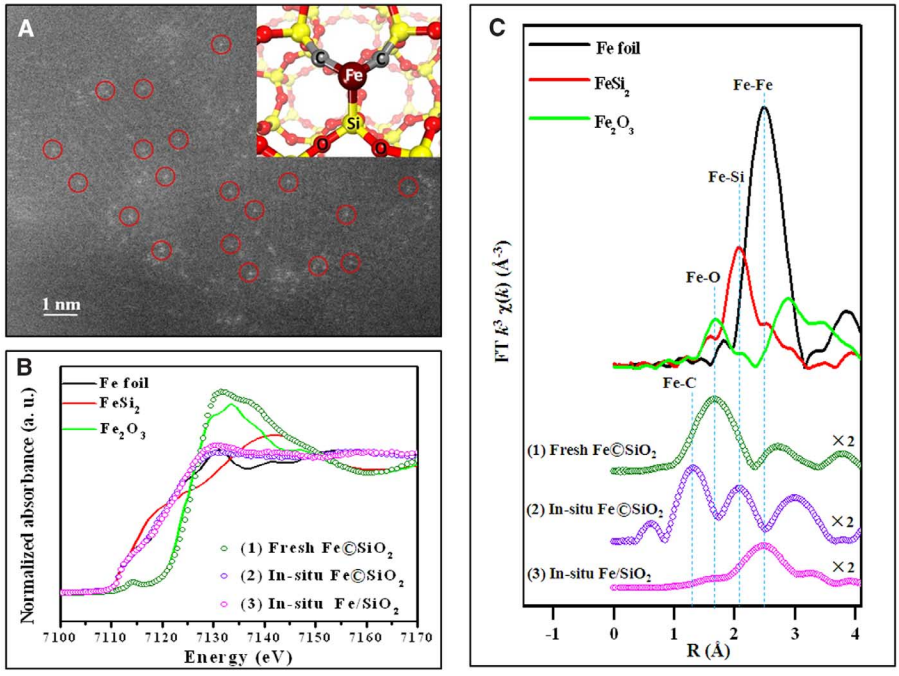

Fig. 2. Structural features of 0.5% Fe©SiO_2. (**A**) STEM-HAADF image of the catalyst after reaction, with the inset showing the computational model of the single iron atom bonded to two C atoms and one Si atom within silica matrix. (**B**) In situ XANES upon activation and (**C**) Fourier transformed (FT) k^3-weighted $\chi(k)$-function of the EXAFS spectra. Solid lines denote reference samples of Fe foil, $FeSi_2$, and Fe_2O_3. Line 1 denotes the fresh 0.5% Fe©SiO_2. Line 2 stands for 0.5% Fe©SiO_2 and line 3 for 0.5% Fe/SiO_2 upon activation in 10% CH_4/N_2 at 1173 K for 2 hours, respectively. R(Å), distance in angstroms.

represented by the signal at mass/charge ratio (m/z) = 15, are clearly observed. Additional signals at m/z = 28, 40, 42, 78, 92, and 128 are assigned to ethylene (C_2H_4), propyne or propadiene (C_3H_4), propylene (C_3H_6), benzene (C_6H_6), toluene (C_7H_8), and naphthalene ($C_{10}H_8$), respectively.

To further elucidate the mechanism, the reaction profile of methyl radicals at 1225 K was simulated with DFT (Fig. 3C and fig. S7) (*22*). Two •CH_3 radicals combine to form C_2H_6 via a strongly exothermic process. C_2H_6 undergoes dehydrogenation readily, giving C_2H_4 and H atoms with an energy barrier of 1.58 eV. By abstraction of H from C_2H_4, the resulting •C_2H_3 radical tends to react with additional C_2H_4 molecules. Further dehydrogenation and cyclization leads to benzene, with an energy barrier of 2.85 eV. C_6H_6 is also readily dehydrogenated by •H and, after further chain growth and cyclization, yields the thermodynamically more stable naphthalene. The low barrier for transformation of C_2H_6 to C_2H_4 explains the absence of C_2H_6 among the experimentally observed products under steady-state reaction conditions, whereas the thermodynamically more stable hydrocarbons C_2H_4, C_6H_6, and $C_{10}H_8$ accumulated and were detected.

At equilibrium at 1225 K and atmospheric pressure, the yields of C_2H_4, C_6H_6, and $C_{10}H_8$ from CH_4 were estimated to be 9.0, 34.0, and 57.0% (*22*), respectively. The relative ratios of these products could be manipulated by changing the reaction conditions. For example, increasing the CH_4 flow rate in the VUV-SPI-MBMS reactor favors formation of C_2H_4 (Fig. 3D), whereas lower flow rates (corresponding to longer residence times) promote cyclization of intermediates leading to aromatics, which are consistent with the GC analysis obtained in the microreactor. These results lend further support to the hypothesis that the reaction is initiated by the catalytic generation of methyl radicals, which subsequently undergo a series of gas-phase reactions. Thus, the conversion efficiency is high, despite the very limited number of surface iron sites and the extremely low surface area of the catalyst.

Heterogeneous systems for CH_4 activation generally still suffer from poor carbon utilization, caused in part by low selectivity. Here, we demonstrate an atom-economical direct CH_4 conversion process, enabled by the lattice-confined single iron sites embedded within a silica matrix, which activate CH_4 and generate methyl radicals. A conversion as high as 48.1% was obtained at 1363 K and a space velocity of 21.4 liter $gcat^{-1}$ $hour^{-1}$, with a selectivity to C_2H_4 of >48.4% (the remainder being aromatics). No deactivation was observed even after reaction for 60 hours, and the total carbon selectivity to the three products remained >99%. Although the dehydrogenation itself is endothermic, high selectivity to ethylene in this process substantially reduces the heat input (estimated to be about half that of a typical thermal pyrolysis process with dominating acetylene in product), as shown in table S3 (*22*). These findings open up new possibilities for fundamental studies of direct, nonoxidative activation of CH_4.

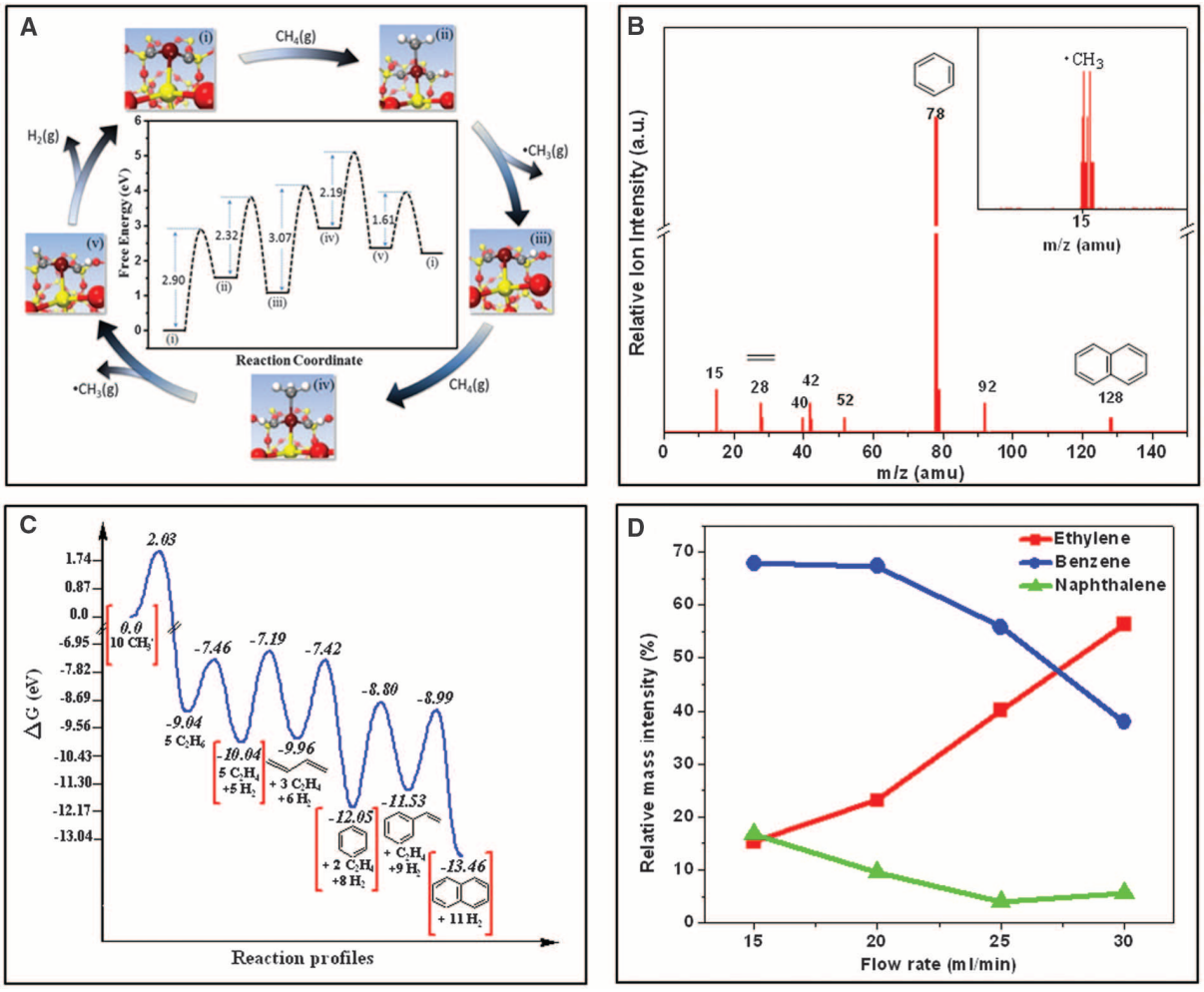

Fig. 3. Investigation of the reaction mechanism over 0.5% Fe©SiO_2. (**A**) DFT calculations on catalytic generation of methyl radicals at 1223 K. (**B**) Species in the reactor effluent at 1193 K, detected by VUV-SPI-MBMS. amu, atomic mass units. (**C**) DFT simulated reaction profile of methyl radicals in the gas phase at 1225 K. ΔG, Gibbs free energy. (**D**) Relative intensity of VUV-SPI-MBMS signals of major products as a function of CH_4 flow rate at 1223 K.

It is anticipated that combining a catalyst such as this one with an efficient reactor technology may enable the development of non–syngas-based routes to transform light hydrocarbons into high–value-added chemicals.

References and Notes

1. www.chemweek.com/lab/ACC-US-chemical-investment-linked-to-shale-gas-reaches-$100-billion_58946.html.
2. J. Li *et al.*, *J. Am. Chem. Soc.* **134**, 836–839 (2012).
3. F. Diederich, *Angew. Chem. Int. Ed.* **52**, 6–7 (2013).
4. H. M. T. Galvis *et al.*, *J. Am. Chem. Soc.* **134**, 16207–16215 (2012).
5. H. M. Torres Galvis *et al.*, *Science* **335**, 835–838 (2012).
6. Note that the construction of two megascale methanol plants in the U.S. Pacific Northwest was recently announced to supply olefin feedstocks to Dalian, China.
7. www.chemweek.com/lab/Chinese-group-plans-two-mega-methanol-plants-in-USPacific-Northwest-to-supply-olefins-feedstock_58289.html.
8. F. P. Larkins, A. Z. Khan, *Aust. J. Chem.* **42**, 1655–1670 (1989).
9. G. E. Keller, M. M. Bhasin, *J. Catal.* **73**, 9–19 (1982).
10. H. Arakawa *et al.*, *Chem. Rev.* **101**, 953–996 (2001).
11. J. H. Lunsford, *Angew. Chem. Int. Ed. Engl.* **34**, 970–980 (1995).
12. S. Arndt *et al.*, *Catal. Rev. Sci. Eng.* **53**, 424–514 (2011).
13. U. Zavyalova, M. Holena, R. Schlögl, M. Baerns, *ChemCatChem* **3**, 1935–1947 (2011).
14. Q. Zhu *et al.*, *Nat. Chem.* **5**, 104–109 (2013).
15. L. S. Wang *et al.*, *Catal. Lett.* **21**, 35–41 (1993).
16. B. M. Weckhuysen, D. J. Wang, M. P. Rosynek, J. H. Lunsford, *J. Catal.* **175**, 338–346 (1998).
17. R. W. Borry, Y. H. Kim, A. Huffsmith, J. A. Reimer, E. Iglesia, *J. Phys. Chem. B* **103**, 5787–5796 (1999).
18. D. J. Wang, J. H. Lunsford, M. P. Rosynek, *J. Catal.* **169**, 347–358 (1997).
19. D. Ma *et al.*, *J. Catal.* **208**, 260–269 (2002).
20. R. Ohnishi, S. T. Liu, Q. Dong, L. Wang, M. Ichikawa, *J. Catal.* **182**, 92–103 (1999).
21. S. Ma, X. Guo, L. Zhao, S. Scott, X. Bao, *J. Energy Chem.* **22**, 1–20 (2013).
22. Supplementary materials are available on *Science* Online.
23. T. V. Choudhary, C. Sivadinarayana, C. C. Chusuei, A. Klinghoffer, D. W. Goodman, *J. Catal.* **199**, 9–18 (2001).
24. M. A. Ermakova, D. Y. Ermakov, A. L. Chuvilin, G. G. Kuvshinov, *J. Catal.* **201**, 183–197 (2001).
25. A. Beloqui Redondo, E. Troussard, J. A. van Bokhoven, *Fuel Process. Technol.* **104**, 265–270 (2012).
26. A. Holmen, O. Olsvik, O. A. Rokstad, *Fuel Process. Technol.* **42**, 249–267 (1995).
27. G. P. Van Der Zwet, P. A. J. M. Hendriks, R. A. Van Santen, *Catal. Today* **4**, 365–369 (1989).
28. H. Schwarz, *Angew. Chem. Int. Ed.* **50**, 10096–10115 (2011).
29. E. W. McFarland, H. Metiu, *Chem. Rev.* **113**, 4391–4427 (2013).
30. B. Qiao *et al.*, *Nat. Chem.* **3**, 634–641 (2011).
31. E. de Smit, A. M. Beale, S. Nikitenko, B. M. Weckhuysen, *J. Catal.* **262**, 244–256 (2009).
32. R. C. Che, L. M. Peng, X. F. Duan, Q. Chen, X. L. Liang, *Adv. Mater.* **16**, 401–405 (2004).
33. X. Pan *et al.*, *Nat. Mater.* **6**, 507–511 (2007).
34. Z. Zhou, H. Guo, F. Qi, *Trends Analyt. Chem.* **30**, 1400–1409 (2011).
35. L. Luo *et al.*, *Sci. Rep.* **3**, 1625 (2013).

Acknowledgments: This work was financially supported by the "Strategic Priority Research Program" of the Chinese Academy of Sciences (grant XDA09030101), the National Natural Science Foundation of China (grants 21321002, 11079005, 21033009, and 21103181), and the Ministry of Science and Technology of China (grants 2011CBA00503 and 2013CB933100). We thank S. L. Scott and H. Metiu for fruitful discussion. An international patent application under the Patent Cooperation Treaty is pending (PCT/CN2013/079977).

Supplementary Materials

www.sciencemag.org/content/344/6184/616/suppl/DC1
Materials and Methods
Figs. S1 to S7
Tables S1 to S3
References (*36*–*66*)

10 March 2014; accepted 15 April 2014
10.1126/science.1253150

Direct, Nonoxidative Conversion of Methane to Ethylene, Aromatics, and Hydrogen

Xiaoguang Guo *et al.*

Science **344**, 616 (2014);
DOI: 10.1126/science.1253150

Science (print ISSN 0036-8075; online ISSN 1095-9203) is published weekly, except the last week in December, by the American Association for the Advancement of Science, 1200 New York Avenue NW, Washington, DC 20005.